Total cross sections for slow-electron (1–20 eV) scattering in solid H_2O

M. Michaud and L. Sanche
Groupe du Conseil de Recherches Médicales en Sciences des Radiations, Faculté de Médecine, Université de Sherbrooke, Sherbrooke, Quebec, Canada J1H 5N4
(Received 30 March 1987)

An analytical method is proposed to determine absolute total cross sections per scatterer and related mean free paths for low-energy electron scattering in disordered molecular solid films. The procedure is based on a two-stream multiple-scattering model of the thickness dependence of the film reflectivity for elastic electrons. The expected analytical behavior and accuracy are tested on a model sample whose scattering properties are generated by a Monte Carlo simulation from initially known parameters. The effects of multiple scattering inside the film and at its interfaces are taken into account and discussed. The thickness dependence of the elastic electron reflectivity of H_2O film condensed at 14 K is reported between 1 and 20 eV incident energy with a spectrometer resolution of 10 meV. The proposed method is applied to extract from these measurements the energy dependence of the total effective and total inelastic cross sections for electron scattering in amorphous ice.

I. INTRODUCTION

The characterization of the electron-solid interaction is of considerable importance for quantitative surface analysis,[1] hot-electron transport,[2] and thermalization distance[3] in polymeric dielectrics as well as for radiation energy deposition in organic and biological materials.[4] This topic has been mainly developed at high energies (i.e., greater than 500 eV) in connection with Auger electron spectroscopy (AES), x-ray photoelectron spectroscopy (XPS), and electron microscopy.[5] At these energies, the interaction of electrons with matter or the energy-loss rate is well described within the first Born approximation. This latter leads readily to the concept of energy- and momentum-dependent dielectric constant or generalized oscillator strength.[5]

The low-energy range (i.e., less than 100 eV) is probed in a number of surface science spectroscopies, namely, electron-energy-loss,[6] ultraviolet-photoelectron,[7] and inverse-photoelectron[8] spectroscopy. At low energy, electrons are known to play a key role in the degradation of high-energy radiation in matter, since in the slowing-down processes of fast electrons, a considerable amount of energy is relayed to electrons of energies smaller than about 100 eV.[4] The behavior of low-energy electrons or hot electrons produced by dielectric breakdown[9] is also of importance, when an insulator is subjected to an intense electric field. With this respect, a series of high-resolution electron-energy-loss (HREEL),[10–12] low-energy electron transmission (LEET),[12–15] and electron-stimulated desorption[16] experiments have been performed on *multilayer* molecular films condensed on a metal substrate. Considering that cross sections for electron-molecule scattering are greater at low energy and that conspicuous effects such as the formation of transient negative ions take place, a quantitative interpretation of the condensed phase results must be extended beyond the Born approximation and must include multiple scattering within and between sites.

The current microscopic theories not being developed to a stage where they can generate the complete energy and angular distribution of electrons scattered from disordered molecular film, we have relied on models based on the solution of the classical transfer equation[11,13,14,17] for the analysis of the experimental results. The apparent difficulty of a classical approach consists in the precise physical interpretation of the macroscopic parameters used to describe the scattering properties of a medium. For instance, one could wonder about the relation between the scattering probability per unit length (SPUL) values or scattering cross sections per scatterer and the microscopic scattering properties of individual components as well as the dynamic structure of the solid. A theoretical investigation which shed more light toward this end, and where a line is drawn between quantum and classical behavior of electron scattering in amorphous condensed matter, has recently been presented by Fano and Stephens.[18] They introduced and defined specifically a stochastic element of probability $k_\varepsilon(\mathbf{q},\omega)$ for energy $\hbar\omega$ and momentum $\hbar\mathbf{q}$ transfer per unit path length to be used in a Boltzmann-type equation.

In surface analysis the quantities of interest are the inelastic mean free path (IMFP) and the attenuation length (AL).[1] The IMFP can be defined in the present context as $1/\alpha_i$, where α_i is the total inelastic SPUL which is related to $k_\varepsilon(\mathbf{q},\omega)$ by $\alpha_i \equiv \int\int_{\omega\neq 0} k_\varepsilon(\mathbf{q},\omega)d\mathbf{q}\,d\omega$. It corresponds to the quantity calculated from the theory at high energy. The AL is more akin to the experimental measurements, in the sense that the IMFP is found to be entangled with elastic and geometrical scattering factors. The most common technique in AL measurements is the overlayer method.[19] This latter is based on the measurement of the attenuation of a photoelectron signal emanating from a substrate as a function of the thick-

ness of a film deposited on that substrate. *The interpretation relies usually on a simple model where elastic multiple-scattering effects are ignored.*[19]

The present work constitutes a first attempt to extract the *energy dependence* of α_i and IMFP in the low-energy range from high-resolution experiments of electrons elastically scattered by disordered solid films. This is achieved by finding particular experimental conditions, under which the multiple-scattering theory previously elaborated[11] simplifies to a simple analytical expression for the thickness dependence of the elastically backscattered intensity. We have chosen to work with multilayer films of amorphous ice formed and held at 14 K. This is the first of two papers aiming to determine energy-loss cross section per scatterer or SPUL values for electron scattering in amorphous ice in the 1–20-eV range. This information should complement the numerous studies[20] intended to evaluate the rate of energy loss or IMFP by high-energy electrons in water, a topic of considerable importance to further develop our understanding of the action of ionizing radiation in biological media.[4]

This paper is organized in the following manner. In Sec. II a simple analytical expression for the elastically backscattered electron intensity is derived from the multiple-scattering model developed in a previous paper[11] (henceforth referred to as I). From this expression a method is elaborated to extract total SPUL or scattering cross-section values from the *thickness dependence* of the *elastic electron reflectivity* of a molecular film deposited on a metal substrate. The method is then tested on a fictitious sample whose elastic electron reflectivity is generated by a Monte Carlo calculation. The effects of elastic multiple scattering within the sample and the film interfaces are thus estimated separately and discussed. The apparatus, the preparation and thickness determination of amorphous films of ice, and the normalization of the scattered intensity scale are described in Sec. III. In Sec. IV we present the results for the energy dependence of the total electron scattering cross section or SPUL values along with the related mean free path (MFP) in amorphous ice. In Sec. V we discuss our data and compare them with SPUL values recently determined[17] at 14 K and 3.2 eV from an N-channel analysis of combined transmission and HREEL spectra, AL values available at 90 K between 18 and 68 eV,[21] and gas-phase data.[22]

II. MODEL AND MEASUREMENT PROCEDURE

We presented in I the derivation of particular analytical expressions for the energy distribution of electrons backscattered from a disordered molecular film (i.e., energy-loss spectra) as a function of its thickness. We started from the transfer equation for plane-parallel problems which implicitly assumes no molecule-substrate interaction and considers a homogenous film growth with no thickness fluctuations. The aim of this section is to develop and to test a procedure for the extraction of the total SPUL or cross section for electron scattering in the film. The method is based on the relation between the elastically scattered intensity and the film thickness.

A. The three-dimensional approach

In order to have a tractable analysis in a three-dimensional (3D) approach, the basis of the procedure can be illustrated first without the effects of the electron reflection from the substrate, the angular deflection at the film-vacuum interface due to the inner potential, and the multiple-scattering processes. In this case *the* 3D *expression* for the elastically backscattered current density $I_1(0,\theta,\phi,E_0)$ at an incident energy E_0 can be given by the expression (5) in I with $E=E_0$, i.e.,

$$I_1(0,\theta,\phi,E_0)=\frac{I_0 Q(\gamma_0,E_0,0)}{\cos\theta[\alpha(E_0)/\cos\theta-\alpha(E_0)/\cos\theta_0]}\times(1-\exp\{-[\alpha(E_0)/\cos\theta_0-\alpha(E_0)/\cos\theta]\}) . \quad (2.1)$$

In this expression γ_0 is the deflection angle between the incident current density (I_0) in direction θ_0,ϕ_0 and the backscattered direction θ,ϕ with respect to the inward normal to the surface. L is the thickness of the film and $Q(\gamma_0,E_0,0)$ is the elastic SPUL per unit solid angle for an electron to be deflected through an angle γ_0. Finally $\alpha(E_0)$ is the total SPUL defined as

$$\alpha(E_0)\equiv\int_{-\infty}^{+\infty}\int_0^{2\pi}\int_1^{-1}Q(\gamma_0,E_0,E-E_0)\times d(\cos\theta)d\phi\,dE ,$$

where $Q(\gamma_0,E_0,E-E_0)$ is the SPUL per unit solid angle, and per unit energy range for an electron of energy E_0 to lose an energy $E-E_0$ and be deflected through an angle γ_0. If we define the elastic reflectivity at a thickness L as $R_1(0,\theta,\phi,E_0)\equiv I_1(0,\theta,\phi,E_0)/I_0$ and that for $L\to\infty$ as

$$R_{1\infty}(0,\theta,\phi,E_0)\equiv R_1(0,\theta,\phi,E_0)\,|_{L\to\infty}=\frac{Q(\gamma_0,E_0,0)}{\cos\theta[\alpha(E_0)/\cos\theta-\alpha(E_0)/\cos\theta_0]} ,$$

then (2.1) can be rewritten as

$$R_1(0,\theta,\phi,E_0)=R_{1\infty}(0,\theta,\phi,E_0)\times\left\{1-\exp\left[-\alpha(E_0)\left[\frac{1}{\cos\theta_0}-\frac{1}{\cos\theta}\right]L\right]\right\} . \quad (2.2)$$

Solving for $\alpha(E_0)$ we get, finally,

$$\ln\left[1-\frac{R_1(0,\theta,\phi,E_0)}{R_{1\infty}(0,\theta,\phi,E_0)}\right]=-\alpha(E_0)\left[\frac{1}{\cos\theta_0}-\frac{1}{\cos\theta}\right]L , \quad (2.3)$$

which indicates that an appropriate semilogarithmic plot of the elastic reflectivity ratio should yield a straight line whose slope is $\alpha(E_0)$. Thus the thickness behavior of the elastic reflectivity is linked to the value of the total SPUL. But one may have concerns about this result since multiple scattering within the film and reflections

at the film interfaces are neglected. In order to evaluate their effects on the final result, let us now compare Eq. (2.3) with the solution of the transfer equation, obtained within the two-stream approximation. Although in this latter the 3D aspect is approximated, it includes exactly contributions arising from multiple-scattering processes, the reflectivity of the substrate, as well as the deflection at the film-vacuum interface.

B. The two-stream approach

With the above assumptions dropped, the energy distribution of the backscattered electron current density resulting from the two-stream approximation of the transfer equation is given by expression (13) in I, i.e.,

$$TJ_r(0,E)=\frac{T}{2\pi}\int_{-\infty}^{+\infty}\frac{I(0,s)R(0,s)}{1-(1-T)R(0,s)}\exp(-isE)ds\ . \tag{2.4}$$

T is the transmission coefficient taking into account the average angular deflection experienced by the electrons which escape the potential barrier set up between the inner-film potential and the vacuum. In the present context it is sufficient to choose T as energy independent. $J_r(0,E)$ is the sum of all fractions of outgoing current density multiply reflected between the film and the potential-barrier interface. Thus $TJ_r(0,E)$ corresponds to the measured quantity. $I(0,s)$ and $R(0,s)$ are the Fourier transform of the incident electron current and of the intrinsic electron reflectivity of the film (i.e., without the effect of the barrier), respectively. The general expression for $R(0,s)$ is given by (9) in I, with the total SPUL defined as

$$\alpha\equiv\int_{-\infty}^{+\infty}[2Q_r(E_0,E-E_0)+Q_f(E_0,E-E_0)]dE\ ,$$

where $Q_r(E_0,E-E_0)$ and $Q_f(E_0,E-E_0)$ are the SPUL per unit energy range for an electron of energy E_0 to lose an energy $E-E_0$, and be deflected in either direction (i.e., large-angle scattering) and only in the forward direction (i.e., small-angle scattering), respectively.

The elastic intensity $TJ_r(0,E=E_0)\equiv J_e^T$ is obtained by substituting in (2.4) the value of $R(0,s)$ by the intrinsic elastic reflectivity $[R(0,s)]_{Q_{re},Q_{fe}}$. This latter corresponds to the first term in the expansion of $R(0,s)$ around the elastic SPUL points Q_{re},Q_{fe} as shown in series (16) of I. If to simplify the notation, we let $I(0,s)\equiv I_0$ and $[R(0,s)]_{Q_{re},Q_{fe}}\equiv R_e$, then (2.4) becomes

$$J_e^T=\frac{I_0TR_e}{1-(1-T)R_e}\ , \tag{2.5a}$$

with R_e given explicitly by

$$R_e=\frac{R_{\infty e}[R_e(L)-1/R_{\infty e}]-(1/R_{\infty e})[R_e(L)-R_{\infty e}]\exp[-\epsilon Q_{re}L(1/R_{\infty e}-R_{\infty e})]}{[R_e(L)-1/R_{\infty e}]-[R_e(L)-R_{\infty e}]\exp[-\epsilon Q_{re}L(1/R_{\infty e}-R_{\infty e})]}\ . \tag{2.5b}$$

In this expression $R_e(L)$ is the elastic electron reflectivity of the substrate located at the position L from the film surface (i.e., position 0). The parameter ϵ is phenomenological and arises from averaging the electron-beam current over all angles in a stream direction. Finally, $R_{\infty e}$ is the intrinsic elastic reflectivity corresponding to the semi-infinite film (i.e., $[R(0,s)]_{Q_{re},Q_{fe}}$ for $L\to\infty$) and is given by the expression (17) in I evaluated at Q_{re},Q_{fe}, i.e.,

$$R_{\infty e}=\frac{1-[1-2Q_{re}/(\alpha-Q_{fe})]^{1/2}}{1+[1-2Q_{re}/(\alpha-Q_{fe})]^{1/2}}\ . \tag{2.5c}$$

Solving Eq. (2.5b) for the factor in the exponential yields

$$\ln\left[\frac{R_e-R_{\infty e}}{R_e(L)-R_{\infty e}}\right]\left[\frac{1/R_{\infty e}-R_e(L)}{1/R_{\infty e}-R_e}\right]=-\epsilon Q_{re}(1/R_{\infty e}-R_{\infty e})L\ . \tag{2.6}$$

By introducing the ratio $R_e/R_{\infty e}$ into the left-hand side and using for the right-hand side the relation $Q_{re}/(\alpha-Q_{fe})=2R_{\infty e}/(1+R_{\infty e})^2$ derived from (2.5c), Eq. (2.6) can be cast into a form similar to Eq. (2.3) as

$$\ln\left[\frac{1-R_e/R_{\infty e}}{1-R_e(L)/R_{\infty e}}\right]+\ln\left[\frac{1-R_eR_{\infty e}}{1-R_e(L)R_{\infty e}}\right]=-2\epsilon(\alpha-Q_{fe})\left[\frac{1-R_{\infty e}}{1+R_{\infty e}}\right]L\ . \tag{2.7}$$

We can make the following observations in comparing Eq. (2.7) with (2.3) and more specifically concerning the effect of the initial assumptions. In the right-hand side of (2.7) the 2ϵ factor can be correlated with the trigonometrical factor appearing in (2.3). The consideration of a *reflectivity for the substrate gives only constant terms which turn out to be irrelevant for the determination of a slope.* Besides the thickness-dependent term $\ln(1-R_eR_{\infty e})$, the elastic multiple-scattering description results in the SPUL Q_{fe} added to the total SPUL α and to the factor $(1-R_{\infty e})/(1+R_{\infty e})$ which renormalizes the $(\alpha-Q_{fe})$ term. The presence of Q_{fe} means that the small-angle elastic scattering does not contribute to the depletion of any electron-beam current. It is peculiar to the two-stream approximation, and the same phenomenology can be found in the Landau formula which is derived when only forward scattering is effective, as shown in the expression (11) in I. Accordingly, this procedure

cannot provide an attenuation parameter corresponding directly to the definition of the total SPUL α and calls for a modified definition. This suggests defining instead the term $(\alpha - Q_{fe})$ as an "effective" total SPUL (α_{eff}) which should lead to α with the knowledge of Q_{fe}. Although it is not possible to determine Q_{fe} and consequently α from the two-stream analysis, α_{eff} can be alternatively used with the determination of $2Q_{re}$ to provide the total inelastic SPUL $(\alpha_i \equiv \alpha - Q_{fe} - 2Q_{re})$. Finally, the potential-barrier transmission coefficient T introduces via Eq. (2.5a) a nonproportional behavior between the measured reflectivity $(R_e^T \equiv J_e^T / I_0)$ and the intrinsic reflectivity R_e of the film.

Hence, without the initial assumptions, the film thickness dependence of the elastically backscattered intensity follows a more complicated behavior than expected from Sec. II A. However, if certain approximations suggested by the experimental context are introduced at this stage, it turns out that a simpler analysis is still possible. In fact, if the reflectivities $R_{\infty e}$, $R_e(L)$, and R_e are such that $R_{\infty e} < 0.1$, $0 < R_e(L)/R_{\infty e} < 3$, and $0 < R_e/R_{\infty e} < 3$, then the second term in the left-hand side of the relation (2.7) can be safely neglected in comparison with the first term. Thus, using $\alpha_{\text{eff}} \equiv \alpha - Q_{fe}$, Eq. (2.7) is reduced to

$$\ln(1 - R_e/R_{\infty e}) - \ln[1 - R_e(L)/R_{\infty e}] = -2\epsilon\alpha_{\text{eff}} L (1 - R_{\infty e})/(1 + R_{\infty e}) . \quad (2.8)$$

In this expression the thickness behavior is now linked only to the value of the intrinsic reflectivity ratio $R_e/R_{\infty e}$. However, as mentioned earlier, it is instead of $R_e/R_{\infty e}$ the ratio $R_e^T/R_{\infty e}^T$ including the effect of the potential barrier which is the measured quantity in an experiment. Using expression (2.5a), it is related to the intrinsic reflectivity ratio $R_e/R_{\infty e}$ by

$$\frac{R_e^T}{R_{\infty e}^T} = \frac{TR_e}{TR_{\infty e}} \left[\frac{1 - (1-T)R_{\infty e}}{1 - (1-T)R_e} \right] . \quad (2.9)$$

By expanding the denominator in large parentheses and applying the experimental conditions stated above with $T \sim 0.5$, it can be shown that the expression in large parentheses is almost equal to 1 with a slight implicit dependence on the thickness pertaining to R_e. Thus Eq. (2.9) can be simplified to

$$R_e^T/R_{\infty e}^T \cong R_e/R_{\infty e} . \quad (2.10)$$

Hence, the effect of the potential barrier turns out to be compensated in first order by the measurement of the reflectivity ratio. Using this latter ratio directly in Eq. (2.8) we obtain, finally,

$$\ln(1 - R_e^T/R_{\infty e}^T) - \ln[1 - R_e(L)/R_{\infty e}] = -2\epsilon\alpha_{\text{eff}} L (1 - R_{\infty e})/(1 + R_{\infty e}) , \quad (2.11a)$$

if $R_e(L) < R_{\infty e}$, or

$$\ln(R_e^T/R_{\infty e}^T - 1) - \ln[R_e(L)/R_{\infty e} - 1] = -2\epsilon\alpha_{\text{eff}} L (1 - R_{\infty e})/(1 + R_{\infty e}) , \quad (2.11b)$$

if $R_e(L) > R_{\infty e}$.

These relations, derived under reasonable restrictions in the multiple-scattering regime, predict a linear behavior for the logarithm of 1 minus the normalized elastic reflectivity as a function of the film thickness, the normalization constant being the reflectivity at infinite thickness. But the meaning of the slope, which was directly related to α in Eq. (2.3), is now modified by the Q_{fe} term and entangled with multiple-scattering effects. These latters arise from the factor $(1 - R_{\infty e})/(1 + R_{\infty e})$ which requires an *absolute intrinsic reflectivity value* $R_{\infty e}$ for its evaluation. Fortunately, this factor is not very sensitive to the value of $R_{\infty e}$; for instance, if $R_{\infty e}$ changes by 100% (i.e., from 0.05 to 0.10), it changes only by 10% (i.e., from 0.90 to 0.82). Thus the measurement of the elastic reflectivity $R_{\infty e}^T$ for the semi-infinite film should be suitable for this purpose considering all other sources of error. Finally, one can see that since the AL is more closely related to the experimental measurements, it can be associated here to the inverse of the entire factor $\alpha_{\text{eff}}(1 - R_{\infty e})/(1 + R_{\infty e})$ in Eqs. (2.11).

C. Test calculation

To test the procedure suggested in Sec. II B, we have simulated an electron scattering experiment with a Monte Carlo calculation[23] using initially known parameters. The prime objective was to verify the analytical behavior of the predicted thickness dependence of the elastic electron reflectivity ratio for scattering *in three dimensions,* and to compare the extracted value of the total SPUL α with the one injected. The parameters were chosen so as to comply with the experiment. The incident energy was fixed at 8 eV. The model sample was characterized by a density similar to the cubic phase of ice at $-130\,^{\circ}\text{C}$ with 3.125×10^{22} molecules cm^{-3},[24] a total scattering cross section per scatterer of 10^{-16} cm^2 (i.e., 0.0568 layer^{-1}), an isotropic elastic scattering cross section per scatterer of 2.2×10^{-17} cm^2 (i.e., 0.0125 layer^{-1}), and an inner potential of 1 eV. The substrate was characterized by an isotropic elastic scattering coefficient of reflectivity equal to 0.15. The incident angle was fixed at $\theta_0 = 14°$ and the calculation of the scattered intensity performed for a small solid angle at $\theta = 135°$ (i.e., $\theta_d = 45°$ with respect to the outward normal). In general the scattered intensity is dependent on θ and ϕ, but for isotropic scattering cross sections it becomes ϕ independent. The calculation was performed by step of 1.76 Å corresponding to the thickness of a layer of ice and from 0 to 54.56 Å (i.e., 0 to 31 layers). The number of events was chosen in order to reduce under $\pm 2\%$ statistic fluctuations in the results.

The ratio $R_e^T/R_{\infty e}^T$ was calculated at each thickness by using the reflectivity at the highest possible thickness (i.e., 31 layers) for $R_{\infty e}^T$. By plotting this ratio minus 1 as a function of the thickness on a semilogarithmic chart as shown in Fig. 1, a straight line was obtained between 0 and 20 layers with a departure from linearity above 20 layers. This latter behavior was predictable, since the value of the reflectivity at 31 layers is slightly higher than that expected for a semi-infinite film and therefore

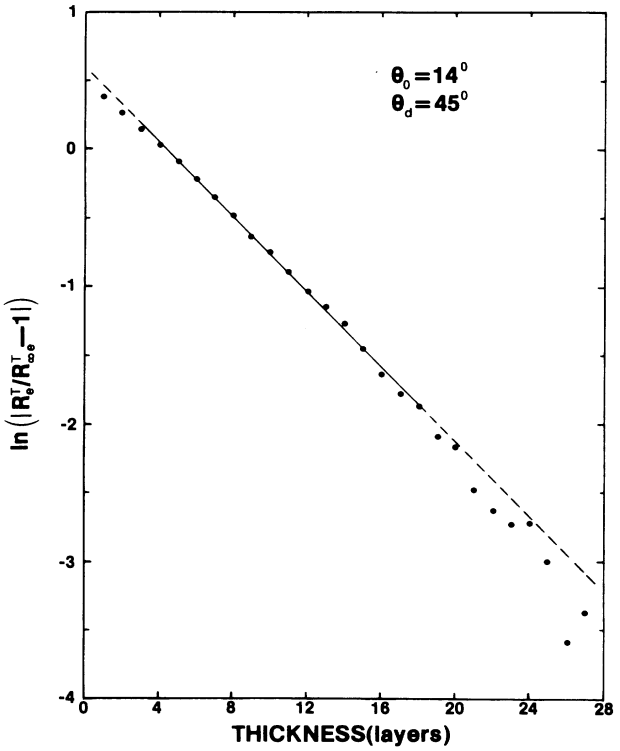

FIG. 1. Semilogarithmic plot of a Monte Carlo simulation (dots) of the normalized elastic electron reflectivity minus 1 as function of the thickness. The normalization constant is taken as the elastic reflectivity at 31 layers. The angle of incident θ_0 and of analysis θ_d has been chosen similar to the experimental configuration. The solid part of the straight line represents the range where a least-square-fit analysis of the data has been performed.

pulls down the curve toward that limit. By applying a standard least-square-fit analysis on these results in the range 3–18 layers, we obtained a correlation coefficient better than 0.998 with a corresponding root-mean-square deviation of $\pm 3.8\%$ for the slope. Using for the parameter ϵ the value 1.22 calculated with the trigonometrical factor in Eq. (2.3), and using to correct for the elastic multiple-scattering effect the factor $(1-R_{\infty e})/(1+R_{\infty e})$ evaluated with the average reflectivity of 0.036 at 31 layers, we were able to retrieve a total cross section of 1.1×10^{-16} cm^2 (i.e., 0.062 layer^{-1}). Owing to the incertitude in the calculation of the slopes, the factor ϵ, and the factor $(1-R_{\infty e})/(1+R_{\infty e})$, the comparison with the true value can be used to evaluate *a posteriori* the accuracy of the method at $\pm 10\%$.

III. EXPERIMENT

A. Apparatus

The apparatus is housed in a bakeable cryopumped ultrahigh-vacuum system[25] (UHV) capable of sustaining working pressures read at the ionization gauge in the mid-10^{-11}-Torr range. The samples to be studied are condensed from gas or vapor phases onto a metal substrate cooled at 14 K. This latter is electrically isolated and press fitted with a ceramic plate to the tip of the cryopump which is mounted on a bellows to allow for X,Y,Z positioning. The gases or vapors initially prepared in a gas-handling manifold are introduced in the system through an *admission valve* which is connected to a small tube having an opening located in front of the cold tip. The manifold consists of two gas- or vapor-inlet sources connected through a bypass and *precision-leak valves* to a small chamber whose volume (180 ml) is precisely known. This calibrated chamber is evacuated by separate adsorption and ion pumping. The absolute pressure of the gases or vapors leaked in or out of this chamber is measured by a capacitance manometer.

The electron scattering measurements were performed with a hemispherical HREEL spectrometer[10] having the following characteristics. With polar coordinates defined relatively to the outward normal of the sample, the polar angle of the monochromator (i.e., the angle of incidence θ_0) can be rotated between 14° and 70° at fixed azimuthal angle. The polar angle of the analyzer (i.e., the angle of analysis θ_d) is fixed at 45° at the opposite azimuth. Double-zoom electron lenses at the output of the monochromator and at the input of the analyzer allow a nearly constant incident current over a wide energy range in the area viewed by the analyzer at the surface of the sample. In the present experiment the combined resolution of the selectors was adjusted at 10 meV full width at half maximum (FWHM) for a corresponding current at the substrate of ~ 0.2 nA. The incident electron energy (E_0) scale was calibrated, within ± 0.1 eV with respect to the vacuum level, by measuring the onset of electron currents transmitted through (i.e., currents measured on the substrate) and scattered from the deposited films.

B. Sample preparation and film thickness measurement

The metal substrate consists of a 2.0×1.0 cm^2 polycrystalline platinum (Pt) ribbon of 0.2 mm nominal thickness supplied by the Ventron Corporation with a stated purity of 99.95%. The ribbon was cleaned by resistive heating in UHV to a temperature of 1500 °C and, in the presence of oxygen, to 900 °C. Energy-loss spectra obtained after these treatments were free from any spurious vibrational losses. Moreover, the energy dependence of the elastically scattered electrons in the specular direction (i.e., 00 beam) indicated according to a recent analysis[26] that the substrate was characterized by (111) microfacets oriented parallel to the surface, but azimuthally disordered. The deposited H_2O films consist of triply distilled water degassed by repeated freeze-thaw cycles under vacuum.

The accuracy in the determination of absolute SPUL or cross-section values is linked to the precision in the measurement of the number of molecules condensed on the substrate. In previous experiments the coverage could be estimated[10] by monitoring the differential pressure drop in the calibrated chamber. Owing to the high

sticking coefficient of water molecules which adsorbed on the small tube and the walls of the manifold, a spurious pressure drop was recorded in the calibrated chamber. Hence, for the present experiment, the previous monitoring was found inaccurate and weakly reproducible. Instead, we developed a procedure by which the transmitted current at the substrate I_S is calibrated against the net pressure drop (ΔP) [i.e., $I_S(\Delta P)$].

This calibration is achieved by establishing initially steady-state conditions of flow in the manifold and the small tube. This is done by opening the admission valve and adjusting the leak valve at the source until the pressure in the chamber is stationary. The vapor is then allowed to flow for about 15 min. Thus we have the relation

$$G+\Delta P/\Delta t+\Delta P_a/\Delta t=0 ,$$

where $\Delta P/\Delta t$ is the net pressure-drop rate, $\Delta P_a/\Delta t$ is the spurious pressure-drop rate, and G is the leak rate from the vapor source. Under these conditions I_S is measured as function of time to yield the curve $I_S(\Delta t)$. This latter is initiated at $t=0$ by a short temperature flash of the substrate. Then the leak valve at the source is closed and the total pressure drop ($\Delta P_T \sim 2\%$) is monitored as function of time, i.e.,

$$\Delta P_T/\Delta t \equiv \Delta P/\Delta t+\Delta P_a/\Delta t .$$

Finally, the admission valve is shut and $\Delta P_a/\Delta t$ is monitored. From these rate measurements the time scale in $I_S(\Delta t)$ is converted into a net pressure-drop scale as $I_S(\Delta P)$, where

$$\Delta P=(\Delta P_T/\Delta t-\Delta P_a/\Delta t)\Delta t .$$

In this manner, the *differential coverage* which is of primary importance for the extraction of *absolute values of the total SPUL or the total cross section* can be accurately determined.

In the next stage of calibration, the net pressure drop (ΔP_{ML}) corresponding to the amount of Ar gas necessary to produce a monolayer on the Pt substrate near 14 K is monitored. The monolayer is identified precisely by observing the amplitude of the quantum-size effect (QSE) as a function of coverage, either in the LEET[15] or in the low-energy elastic specular intensity.[27] The amplitude of the interference for a monolayer saturates before other structures related to additional layers appear.

Finally, ΔP_{ML} is related to the density of a monolayer (d_{ML}) of Ar on Pt and then used to convert the ΔP scale of the $I_S(\Delta P)$ curve for H_2O into a surface-density scale (Δd) (i.e., molecules cm^{-2}) with $\Delta d=(d_{\mathrm{ML}}/\Delta P_{\mathrm{ML}})\Delta P$, assuming the same sticking coefficient. The formation of a hcp structure near the monolayer coverage seems to be a general property of noble-gas-adsorption systems,[28,29] which manifests the relatively weak interaction between the inert-gas atoms and the surface underneath. The packing density of Ar adsorbed on various substrates corresponds to a hcp cell parameter lying[28] generally between 3.7 and 3.95 Å. These values compare favorably with the Ar-Ar distance at 3.76 Å in the (111) plane of bulk Ar at 20 K.[30] Since there is no available data on Pt(111), the monolayer coverage can be reasonably chosen as equal to the latter density, with $d_{\mathrm{ML}}=8.167\times10^{14}$ atoms cm^{-2}.[30]

Since the measurement of the transmitted current as function of time is an accurate step, the major incertitude is found in pressure measurements ($\pm5\%$) and in the value chosen for the (111) plane density of Ar on Pt ($\pm5\%$). When combined in the Δd formula, these latters lead to an incertitude of $\pm15\%$ on the value of the molecular coverage. The H_2O coverage can be converted for convenience into a number of layers by using the density 5.72×10^{14} molecules cm^{-2} of the (111) face of the cubic form of ice at $-130\,^{\circ}\mathrm{C}$.[24]

To control our calibration, we measured in a different type of experiment LEET spectra in the 0–20-eV range as function of time during warming up of a 40-layer H_2O film on the Pt substrate. As function of time, a break in the transmitted intensity was observed for several incident energies and attributed to a change either in the desorption rate or in the crystalline structure of the remaining condensate near the metal surface. By looking for the value of the transmitted current at the break point, we were able to deduce with our calibration a corresponding coverage of 1.03×10^{15} molecules cm^{-2} which is equivalent to 1.82 layers, if the density of H_2O adsorbed on Pt(111) at 5.65×10^{14} molecules cm^{-2} is used.[31] This finding correlates well with the formation of an ordered bilayer of ice around 180 K, as described by several recent electron-stimulated desorption and vibrational spectroscopic studies of H_2O adsorbed on Ru(001) (Ref. 32) and Pt(111).[33]

We assume for the extraction procedure and the thickness calibration that a film grows homogeneously (i.e., constant density) as well as with a uniform thickness. In practice, several types of film growth have been observed and mechanisms proposed, particularly in relation with studies of epitaxial growth on single crystals.[34] The three major types are the layer-by-layer growth (Frank van der Merve), the isolated-island growth (Volmer-Weber), and the mixed growth involving initially the formation of a monolayer followed by an island growth (Stranski-Krastanov). Which type is favored depends mainly on structural effects and how the strain energy is distributed inside the deposited film as well as between the film and the metal substrate. For water vapor condensed on a Pt(111) substrate, LEED investigations[31] conducted below 125 K indicate the formation of disordered ice layers independent of the vapor flux. From x-ray diffraction studies it has been inferred that water vapor condensed at a deposition rate of 4–10 mg h^{-1} on a cold substrate grows at 77 K into a low-density amorphous form at 0.94 g cm^{-3} or at 10 K into high-density amorphous form at 1.1 g cm^{-3}.[35] However, it has been suggested shortly after that the high-density form is more difficult to obtain, since it seems to depend on nucleation steps and that under most slow-rate depositions the low-density form is more likely to occur.[36] From these considerations we believe that for the first few layers the density of our ice films may vary due to the proximity of the substrate. However, owing to the deposition

rate (less than 0.004 mg cm^{-2} h^{-1}) used in this experiment, the density for the subsequent layers should become constant and typical of the low-density amorphous form of ice. Variations in film thickness are not expected to be too serious as long as they are smaller than the mean free path.

C. Backscattered intensity normalization

Prior to a two-stream analysis an absolute reflectivity scale is established for the experimental backscattered electron intensity in the following manner. From the law of current conservation it is shown in the Appendix that under certain reasonable conditions we have between the transmitted current I_S and the backscattered current per unit solid angle $J(\theta_d)$ the following relation:

$$\frac{I_S}{I_0}+\frac{J(\theta_d)}{I_{0,d}}=1 \ . \tag{3.1}$$

In this equation I_0 is the incident current impinging at a particular angle θ_0 on the surface of a film and $I_{0,d}$ is an effective incident current related to the differential backscattered current at a particular angle of analysis θ_d. However, with this apparatus, it is not possible to measure directly either I_0 or $I_{0,d}$. Instead a full energy-loss spectrum $J(E,\theta_d)$ (i.e., from threshold to the incident energy) along with the transmitted current I_S are recorded either for various incident energies or several thicknesses. By plotting I_S versus $J(E,\theta_d)$ once integrated from threshold to the incident energy to retrieve $J(\theta_d)$ a straight line is obtained whose extrapolated ends intercept the ordinate and abscissa axes at I_0 and $I_{0,d}$, respectively. The $I_{0,d}$ parameter can be alternatively visualized or interpreted as the incident electron current backscattered in a particular direction by an ideal medium whose total electron reflectivity is equal to 1 (i.e., where all incident electrons are finally scattered out of the film). Thus by normalizing the scattered intensity scale of an energy-loss spectra by this effective incident current as

$$\frac{J(E,\theta_d)}{I_{0,d}}\equiv R(E,\theta_d) \ , \tag{3.2}$$

the energy integral of an elastic or inelastic feature can be expressed in terms of an elastic or inelastic absolute reflectivity value. As long as the angular distribution of the backscattered electron intensity does not change too much as a function of the incident energy or thickness, this method provides an experimental reflectivity scale convenient for comparison with two-stream calculations.

IV. RESULTS

A. Measurement of the elastic electron reflectivity

Measurements of the elastically backscattered electron intensity were monitored at various angles of incidence θ_0 between 14° and 70°, and at an angle of analysis $\theta_d=45°$, with respect to the outward normal of the surface. The incident energy E_0 was swept by step of 1 eV between 1.2 and 19.2 eV. In Fig. 2 the energy dependence of the elastic reflectivity at $\theta_0=14°$ for H_2O condensed at 14 K is presented for several film thicknesses. The curve labelled 0 represents the elastic reflectivity of the Pt substrate in the off-specular direction, and is about two orders of magnitude smaller than that in the specular direction. The reflectivity for the adlayers is found to be weakly dependent on the incident angle θ_0 above eight layers. From that thickness two maxima develop and only a decrease in the overall intensity is observed for increasing coverage. Film charging limited measurements to 40 layers. Since we preferred to collect the maximum signal on a large energy range, the transmission of the spectrometer optics particularly at low energy is uncertain. This is not a serious problem because most of the analysis relies on the reflectivity ratio as explained previously. With the normalization procedure of Sec. III C, the elastic reflectivity in the 40-layer curve is estimated around 6% and 7.5% for the first and second maximum, respectively. It should be noted that any imprecisions in the absolute reflectivity are to be minimized in the $(1-R_{\infty e})/(1+R_{\infty e})$ factor of Eqs. (2.11).

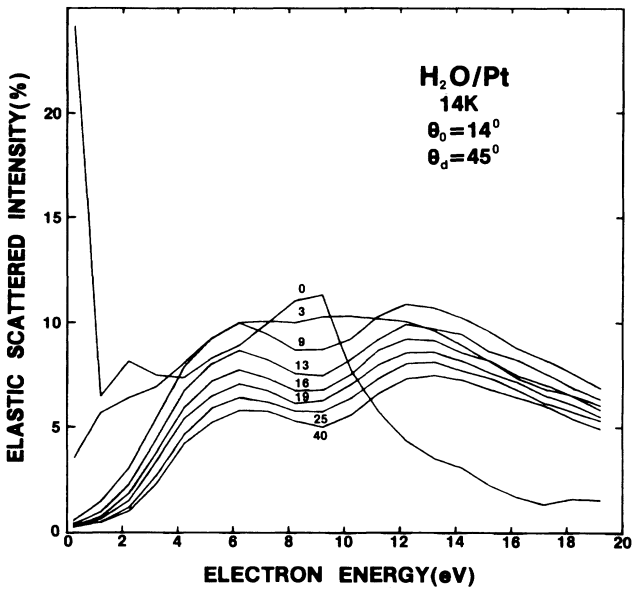

FIG. 2. Measurement of the elastic scattered electron intensity as a function of the incident energy for various thicknesses of amorphous films of ice condensed on a polycrystalline Pt substrate. The angle of incidence (θ_0) and of analysis (θ_d) are 14° and 45°, respectively, with respect to the outward normal of the surface. The numbers near each curve indicate the thickness of the film in layers. The intensity scale is calibrated in absolute reflectivity by the normalization procedure explained in the text.

B. Total effective and total inelastic scattering cross section per scatterer

According to the finding of Sec. II, the plot of the $\ln(|R_e^T/R_{\infty e}^T-1|)$ term in Eqs. (2.11) versus coverage for a particular electron energy should yield a straight line. The slope (b) is related to the total effective SPUL

(α_{eff}) by

$$b = 2\epsilon\alpha_{\text{eff}} L(1 - R_{\infty e})/(1 + R_{\infty e}) , \quad (4.1a)$$

if the coverage is expressed in units of length (i.e., layer), or to the total effective-scattering cross section per scatterer ($\sigma_{T,\text{eff}} \equiv \alpha_{\text{eff}}/n$) by

$$b = 2\epsilon\sigma_{T,\text{eff}} nL(1 - R_{\infty e})/(1 + R_{\infty e}) , \quad (4.1b)$$

if the coverage is expressed in unit of surface density (nL), with n the bulk density of the sample. Owing to the coverage calibration of Sec. III B, it is $\sigma_{T,\text{eff}}$ in (4.1b) which is to be directly extracted from the measurements.

In Figs. 3(a) and 3(b) we present for several incident energies the semilogarithmic plots of the elastic reflectivity ratio using the 40-layer curve as semi-infinite data. For all these plots a good linear behavior can be observed for a coverage above 5×10^{15} molecules cm^{-2} (i.e., eight layers) despite some dispersion in the data above 20 layers. The departure from the linear behavior at low thicknesses is partly attributed to the anisotropic reflectivity of the substrate and to that of the first few layers. These reflectivities are characterized by a pronounced specular component. Also, this could be attributed to modifications in the growth mode of the first few layers in matching the surface of the substrate with the amorphous form of the bulk.

In Fig. 4 the open dots joined by the continuous curve represent the total effective-scattering cross section [$\sigma_{T,\text{eff}} = (\alpha - Q_{fe})/n$] as a function of incident energy. This latter leads directly to the total scattering cross section ($\sigma_T \equiv \alpha/n$) if the small-angle elastic SPUL component (Q_{fe}) is zero. Each point results from the average value of the slopes b computed after two runs, then corrected for the ϵ parameter and the energy dependence of the multiple-scattering factor according to Eq. (4.1b). The ϵ parameter is chosen constant in energy and equal to the trigonometrical factor evaluated at the experimental configuration, as in the Monte Carlo simulation. The multiple-scattering factor could be evaluated in a first approximation with the 40-layer reflectivity measurement ($\sim R^{T}_{\infty e}$) shown in Fig. 2. Instead, it is calculated more consistently with the corresponding intrinsic elastic reflectivity ($R_{\infty e}$) represented by the dashed curve in Fig. 4. The origin of this latter is to be discussed shortly. The error bar associated with each open dot represents plus and minus the root-mean-square deviation of a slope value which results from a standard least-square fit of a straight line to the data. It does not include the systematic uncertainty dependent on the coverage measurement (i.e., nL), the ϵ parameter, or the multiple-scattering factor. We can attribute for these latter two, as seems to indicate the fit to the data generated by the Monte Carlo simulation, a combined error of $\pm10\%$. With the additional error of $\pm15\%$ originating from the thickness measurement a value of $\pm25\%$ is

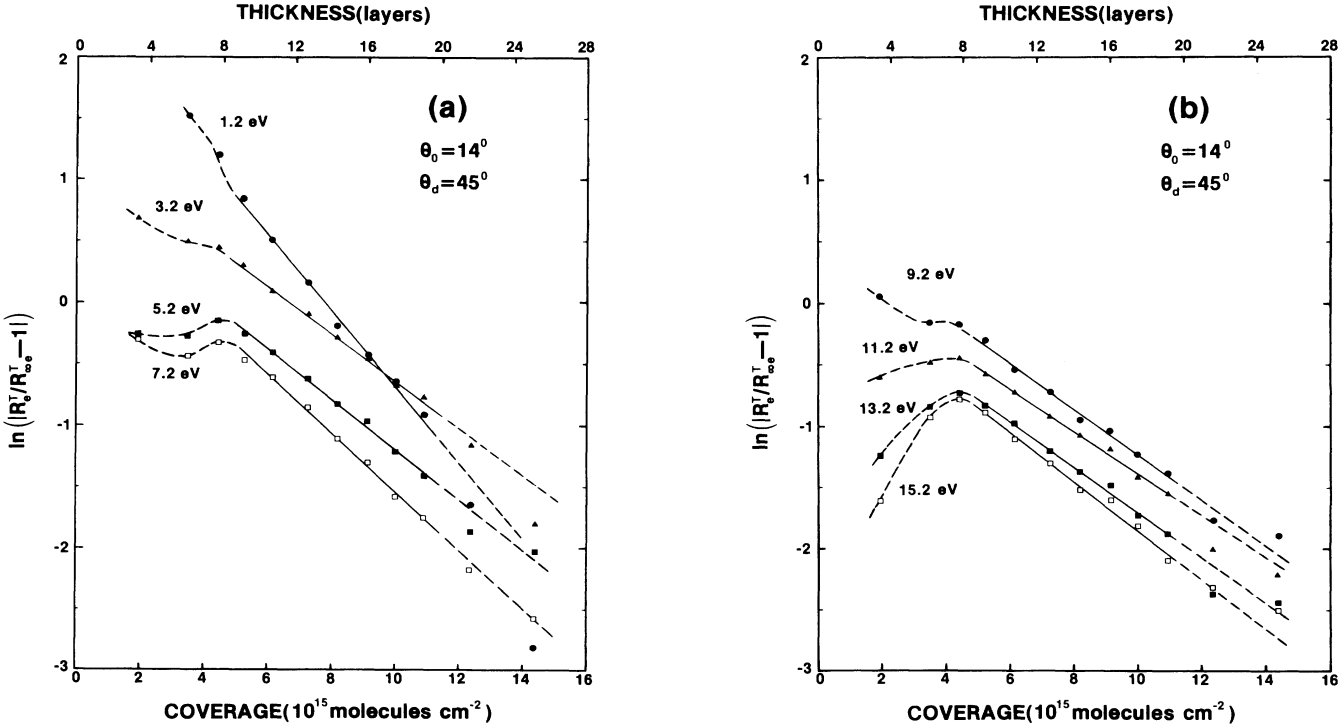

FIG. 3. (a),(b) Semilogarithmic plot of the normalized elastic electron reflectivity minus 1 as a function of film thickness for various incident electron energies. The normalization constant for each energy is taken as corresponding to the elastic reflectivity at 40 layers. This latter proves to be reasonably close to the elastic reflectivity of the semi-infinite film $R^{T}_{\infty e}$. Each straight line results from a least-square-fit analysis of the data comprised between 8 and 20 layers coverage (continuous part) and its slope is related to the electron total effective and total inelastic-scattering cross section per scatterer.

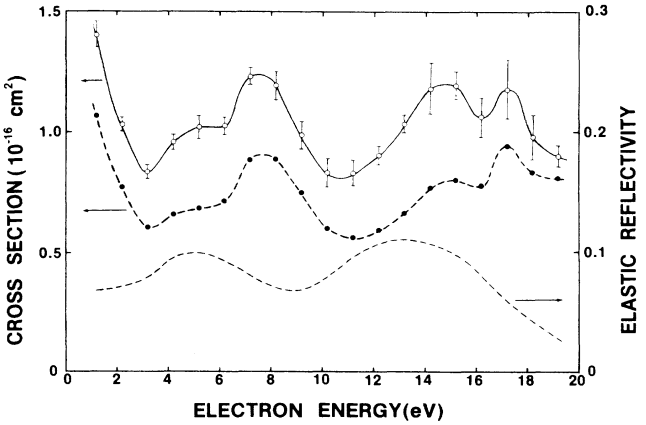

FIG. 4. The open-dot solid curve is the energy dependence of the total effective cross section per scatterer [$\sigma_{T,\text{eff}} \equiv (\alpha - Q_{fe})/n$] for electron scattering in amorphous ice. The dashed curve represents the intrinsic (i.e., without the effect of the film-vacuum potential barrier) elastic electron reflectivity of a semi-infinite film of amorphous ice (see text). It is related to the isotropic elastic-scattering cross section by Eq. (4.3). The combination of this latter with $\sigma_{T,\text{eff}}$ through Eq. (4.2) leads to the total inelastic-scattering cross section per scatterer $\sigma_{T,i}$ shown by the dot-dashed curve.

finally obtained for the total systematic uncertainty. Of course, this has little effect on the relative values of $\sigma_{T,\text{eff}}$ and should scale either up or down our results.

The dot-dashed curve in Fig. 4 represents the total inelastic-scattering cross section ($\sigma_{T,i} \equiv \alpha_i/n$). Since $\sigma_{T,\text{eff}}$ corresponds also to the contribution of the large-angle elastic SPUL ($2Q_{re}$) plus the total inelastic SPUL (α_i) [i.e., $\sigma_{T,\text{eff}} = (2Q_{re} + \alpha_i)/n$], $\sigma_{T,i}$ is calculated through the following relation:

$$\sigma_{T,i} = \sigma_{T,\text{eff}}(1 - 2Q_{re}/\alpha_{\text{eff}}) , \tag{4.2}$$

with the knowledge of the ratio $2Q_{re}/\alpha_{\text{eff}}$. This latter ratio is obtained with an average accuracy of $\pm 4\%$ by a procedure based on a two-stream analysis of several energy-loss spectra,[11] which will be described in detail in a forthcoming paper.[37] Furthermore, this ratio is also at the origin of the $R_{\infty e}$ curve through the expression (17) in I evaluated at Q_{re}, Q_{fe}, i.e.,

$$R_{\infty e} = \frac{1 - (1 - 2Q_{re}/\alpha_{\text{eff}})^{1/2}}{1 + (1 - 2Q_{re}/\alpha_{\text{eff}})^{1/2}} . \tag{4.3}$$

The uncertainty on $R_{\infty e}$ is $\pm 5\%$ and results in a value less than $\pm 1\%$ for the factor $(1 - R_{\infty e})/(1 + R_{\infty e})$, because of the compensating effect mentioned in relation with Eqs. (2.11). In Table I we give the numerical values for $\sigma_{T,\text{eff}}$ and $\sigma_{T,i}$, along with computed MFP values using the bulk density of low-density amorphous ice at 3.15×10^{22} molecule cm^{-3}.[35]

V. DISCUSSION

Since the present method is based on an analysis[11] where only the average backscattered electron elastic intensity is considered (i.e., the detail of the angular distribution is neglected), it cannot provide a value corresponding to the total scattering cross section (σ_T). Instead, it yields a total effective-scattering cross section ($\sigma_{T,\text{eff}}$) which differs from σ_T only by the value of the small-angle elastic SPUL component. In practice, this latter occurs to be effectively transparent to the electron-beam attenuation. As such, $\sigma_{T,\text{eff}}$ is applicable to various transport problems. For example, $\sigma_{T,\text{eff}}$ can be related to the elastic transmission through a slab of matter (i.e., electron having undergone only elastic scattering and so still available for energy-deposition processes). This is readily achieved in the two-stream approximation by solving the Eqs. (8) of I for the transmitted current instead of the reflectivity. This transport property when measured as function of the film thickness constitutes the basis of the overlayer method of AL measurements.[19] Moreover, $\sigma_{T,\text{eff}}$ is central to the extraction of the cross sections per scatterer for the major energy-loss processes. As will be shown in a forthcoming paper,[37] by using the two-stream model of I to fit numerically the energy distribution of a HREEL spectrum of a sufficiently thick film, the relative magnitude (i.e., with respect to $\sigma_{T,\text{eff}}$) of the cross sections can be obtained. By resuming this analysis for several incident energies and normalizing with $\sigma_{T,\text{eff}}$, the energy dependence of the individual cross sections can be obtained. Furthermore, $\sigma_{T,\text{eff}}$ leads readily to the value of the total inelastic-scattering cross section ($\sigma_{T,i}$) which is more relevant for the characterization of the energy transferred by an electron to a medium. For amorphous ice, we find that $\sigma_{T,\text{eff}}$ is on the average 30% greater than $\sigma_{T,i}$ in the 1–20-eV energy range. Hence, the isotropic (i.e., large-angle) component of the elastic-scattering cross section can also be important for the electron-beam attenuation in ice. However, this effect is expected to be partially compensated in AL measurements by elastic multiple scattering, as can be seen in Eqs. (4) from the contribution of the factor $0.8 < (1 - R_{\infty e})/(1 + R_{\infty e}) < 0.9$.

Comparisons of $\sigma_{T,\text{eff}}$ with other available data for ice can only be made for the low and high end of our energy range. At low energy, Bader *et al.*[17] have proposed to extract various SPUL values from a method based on a N-channel analysis of HREEL data for a film at high thickness combined with LEET measurements as a function of film thickness. They have obtained for similarly grown film of amorphous ice an average total SPUL of 0.085 layer^{-1} in the 0–3.2-eV range. This can be compared to our total effective-scattering cross section or corresponding SPUL values of 0.080, 0.059, and 0.047 layer^{-1} at 1.2, 2.2, and 3.2 eV, respectively. As such, a LEET measurement corresponds intuitively to the electron current collected by the metal substrate. This transport property can be alternatively and better visualized from the point of view of the electron current backscattered from the target and able to escape the potential-barrier interface. In other words, a LEET spectrum can be seen to result from the complement of the total electron reflectivity (i.e., angularly and energetically integrated) of the target. Thus, in order to describe a LEET spectrum—for instance, in the two-stream

TABLE I. Total effective $\sigma_{T,\text{eff}}$ and total inelastic $\sigma_{T,i}$ cross section per scatterer (10^{-16} cm^2) with the corresponding $1/\alpha_{\text{eff}}$ and $1/\alpha_i$ MFP values (Å) for electron scattering in the low-density amorphous form of ice.

Electron energy (eV)	$\sigma_{T,\text{eff}}$	$1/\alpha_{\text{eff}}$	$\sigma_{T,i}$	$1/\alpha_i$	Gas[a]
1.2	1.40	22.7	1.06	30.0	0.74
2.2	1.03	30.8	0.77	41.2	0.46
3.2	0.83	38.2	0.61	52.0	0.46
4.2	0.96	33.1	0.65	48.8	0.55
5.2	1.02	31.1	0.68	46.7	0.61
6.2	1.02	31.1	0.70	45.3	0.66
7.2	1.23	25.8	0.88	36.1	0.68
8.2	1.18	26.9	0.89	35.7	0.65
9.2	0.98	32.4	0.75	42.3	0.57
10.2	0.82	38.7	0.60	52.9	
11.2	0.83	38.2	0.56	56.7	
12.2	0.90	35.3	0.59	53.8	
13.2	1.03	30.8	0.66	48.1	
14.2	1.18	26.9	0.76	41.8	
15.2	1.19	26.7	0.80	39.7	
16.2	1.05	30.2	0.77	41.2	
17.2	1.17	27.1	0.94	33.8	
18.2	0.97	32.7	0.82	38.7	
19.2	0.90	35.3	0.81	39.2	

[a]The gas-phase values correspond to the sum of cross sections for the stretch and bending modes of H_2O taken from Seng and Linder (Ref. 22).

approximation—we need simultaneously the energy dependence of the forward and backward components of the cross sections for the major energy losses as well as the potential-barrier transmission coefficient. Therefore, a fit of LEET spectra as a function of the film thickness becomes a multiple task and is particularly dependent on the value chosen for the potential-barrier transmission coefficient. Alternatively, the elastically backscattered intensity ratio is almost independent from this latter coefficient and leads more directly to $\sigma_{T,\text{eff}}$. Nevertheless, a good agreement between the measured and calculated LEET spectrum is needed *a postiori* to assess the overall consistency of the parameters.

At higher energy, the only other avaiable data come from the AL measurements of Kurtz *et al.*,[21] performed in the 18–68-eV range for ice held at 90 K. They give at 18 eV an AL of 18.2 Å±35% which compares, within experimental incertitudes, with our values 26 and 30.4 Å±35% at 17.2 and 18.2 eV, respectively. These latter numbers differ from those in Table I, because the correction arising from the multiple-scattering factor in Eqs. (4.1) was neglected in order to compare with values extracted from the overlayer method, where elastic multiple scattering is not taken explicitly into account.

The most recent published gas-phase results on measurements of the total cross section for electron-H_2O scattering which covers our energy range is that of Szmytkowski.[38] This work includes also comparisons between recent and previous data in this field.[39] Although there is a certain discrepancy between the magnitude of the cross sections originating from various sources, there is a good agreement with respect to their general behavior. Total cross sections rise sharply below 3 eV and show a broad maximum around 9 eV. However, the comparison between the total scattering cross sections measured in the gas and extracted in the solid phase cannot be made too directly, because the various nuclear and electronic excitation modes of an isolated molecule are coupled in the condensed phase. For instance, owing to the strong hydrogen bonding in condensed H_2O, the rotational and translational degrees of freedom of the molecules become hindered, whereas the intramolecular-vibrational modes are considerably perturbed. Furthermore, owing to the quantum properties of the electron, cross sections for electron scattering in solid, which are extracted from any classical analysis, are subjected to include intrinsically correlation effects related to the proximity of scattering sites. Hence, for an amorphous solid an effective volume can be defined whose linear dimension cannot be smaller than the electron wavelength, and beyond which a classical transport equation is expected to work. This effective volume should reduce to the size of a volume occupied by a molecule as in to the gas phase, only at sufficiently high energy and for disordered medium.

Keeping in mind these concepts, we included in Table I the sum of the intramolecular-vibrational cross sections for electron-H_2O scattering between 1.2 and 9.2 eV measured by Seng and Linder[22] for comparison with $\sigma_{T,i}$. Although $\sigma_{T,i}$ include additionally the cross sections for electron-exciting hindered rotations and translations as well as electronic states above 7.2 eV, our values compare reasonably with those from the gas-phase data and follow the same general trend. The features appearing in

the $\sigma_{T,\text{eff}}$ and $\sigma_{T,i}$ curves of Fig. 4 can be better analyzed with the knowledge of the individual excitation cross sections. These latters are obtained and discussed at length in a forthcoming article.[37] We summarize here the key results for the sake of completeness. The difference between $\sigma_{T,\text{eff}}$ and $\sigma_{T,i}$ is, according to Eq. (4.2), the isotropic component of the elastic cross section per scatterer $(2Q_{re}/n)$. It is characterized by two broad maxima located at 6 and 14.5 eV. These latter features being correlated with two maxima in the structure factor of amorphous ice[35] suggest *a priori* that they could originate from interference effects. The rise at low energy in $\sigma_{T,i}$ is due to cross sections for electron-exciting hindered translations and rotations and can be explained[37] by various direct scattering processes (i.e., electron-dipole and electron-polarization interaction).[40] The feature around 7 eV in $\sigma_{T,i}$ originates mainly[37] from the sum of the cross sections for electron exciting the stretching modes as well as the hindered translations and rotations. These features are ascribed[37] to the formation of the molecular anion states $^2B_1$,$^2B_2$ (i.e., resonance scattering) known to exist in this energy range from the gas-phase data.[22,41,42] Finally, the rise above 11 eV in $\sigma_{T,i}$ is attributed mainly[37] to the total cross section for excitation of various electronic processes and reaches 37% of $\sigma_{T,i}$ at 17 eV. Although the uncertainty is larger in this energy range, the two maxima which can be observed around 15 and 17 eV could tentatively be correlated with the features found in vacuum-ultraviolet absorption spectra of ice around 14.5 and 17.5 eV, respectively.[43] This latter feature is associated with electronic transition of intramolecular type whereas the former seems to be due to electronic transitions sensitive to the crystalline field.[43]

VI. SUMMARY

We have shown that the multiple-scattering theory previously elaborated[11] could yield under certain approximations a formula relating a total effective-scattering cross section $\sigma_{T,\text{eff}}$ to the thickness dependence of the elastic electron reflectivity of a film condensed on a substrate. This cross section is the sum of the large-angle elastic- and of all inelastic-scattering cross sections $\sigma_{T,i}$. The ability of this formula to retrieve fundamental scattering parameters was first tested in a Monte Carlo simulation. Afterwards, the experimental conditions under which this prescription applies were found for electron scattering from condensed H_2O, and the associated total cross sections were obtained at 1 eV intervals between 1–20 eV of incident energy. The extracted $\sigma_{T,\text{eff}}$, $\sigma_{T,i}$ and corresponding MFP are listed in Table I. The overall accuracy is ±35% of the quoted numbers.

ACKNOWLEDGMENTS

We wish to thank T. Goulet for having kindly agreed to perform the Monte Carlo calculation. Financial support from the Medical Research Council of Canada is gratefully acknowledged.

APPENDIX: RELATION BETWEEN THE TRANSMITTED AND BACKSCATTERED INTENSITIES

Consider an incident electron current I_0 impinging on a film at angles θ_0,ϕ_0 with respect to the inward normal of the surface. By conservation of currents, we have between the transmitted current I_S and the backscattered current per unit solid angle and per unit energy range $J(E,\theta,\phi)$ the relation

$$I_0 = I_S + \int_0^{2\pi}\int_{\pi/2}^{\pi}\int_0^{E_0} J(E,\theta,\phi)\,dE\,\sin\theta\,d\theta\,d\phi\ , \tag{A1}$$

The integration limits are between threshold and the incident energy E_0 and for the half-angular space. Performing the integration on the energy (A1) becomes

$$I_0 = I_S + \int_0^{2\pi}\int_{\pi/2}^{\pi} J(\theta,\phi)\sin\theta\,d\theta\,d\phi\ , \tag{A2}$$

where $J(\theta,\phi)$ corresponds to the differential backscattered current. The angular distribution of this latter can be expressed relative to a particular direction θ_p,ϕ_p as

$$\begin{aligned} J(\theta,\phi) &= J(\theta_p,\phi_p) + J'(\theta-\theta_p,\phi-\phi_p) \\ &= J(\theta_p,\phi_p)\left[1+\frac{J'(\theta-\theta_p,\phi-\phi_p)}{J(\theta_p,\phi_p)}\right], \end{aligned} \tag{A3}$$

where $J'(\theta-\theta_p,\phi-\phi_p)$ is the variation of the backscattered current expressed relative to the value $J(\theta_p,\phi_p)$.

Once (A3) is inserted in (A2) and the angular integration carried out, it yields

$$I_0 = I_S + J(\theta_p,\phi_p)\left[4\pi+\frac{J'_T(\theta_p,\phi_p)}{J(\theta_p,\phi_p)}\right], \tag{A4}$$

where

$$J'_T(\theta_p,\phi_p) \equiv \int_0^{2\pi}\int_{\pi/2}^{\pi} J'(\theta-\theta_p,\phi-\phi_p)\sin\theta\,d\theta\,d\phi\ .$$

If $J'_T(\theta_p,\phi_p)$ is proportional to $J(\theta_p,\phi_p)$, i.e.,

$$J'_T(\theta_p,\phi_p)/J(\theta_p,\phi_p) \equiv a(\theta_p,\phi_p)\ ,$$

or in other words if the angular distribution is independent of the intensity of $J(\theta_p,\phi_p)$, then (A4) can be considered as a linear equation

$$I_0 = I_S + J(\theta_p,\phi_p)[4\pi + a(\theta_p,\phi_p)]\ . \tag{A5}$$

The evaluation of this equation for $J(\theta_p,\phi_p)=0$ provides $I_S=I_0$, while for $I_S=0$ it yields

$$J(\theta_p,\phi_p) = I_0/[4\pi + a(\theta_p,\phi_p)] \equiv I_{0,p}\ .$$

This latter relation allows (A5) to be written in the form

$$1 = \frac{I_S}{I_0} + \frac{J(\theta_p,\phi_p)}{I_{0,p}}\ , \tag{A6}$$

where $I_{0,p}$ is defined as an effective incident current particular to the measurement of the backscattered current in the direction θ_p,ϕ_p. For an isotropic angular distribution $I_{0,p}$ is given by $I_0/4\pi$ as expected. If in order to comply with the experimental configuration, the angle of

analysis is fixed in the azimuthal plane of the incident beam (i.e., $\phi_p = \phi_0$), and is redefined with respect to the outward normal of the film with $\theta_d = \pi - \theta_p$, then (A6) can be rewritten finally as

$$1 = \frac{I_S}{I_0} + \frac{J(\theta_d)}{I_{0,d}} \ . \tag{A7}$$

[1]A. L. Tofterup, Phys. Rev. B **32**, 2808 (1985) and references cited therein; C. J. Powell, Scanning Electron Microsc. **4**, 1649 (1984) and references cited therein.

[2]T. Hibma, P. Pfluger, and H. R. Zeller, in *Electronic Properties of Polymers and Related Compounds,* Vol. 63 of *Springer Series in Solid-State Sciences* (Springer, New York, 1985); E. Cartier and P. Pfluger, Phys. Rev. B **34**, 8822 (1986).

[3]N. Gee and G. R. Freeman, Phys. Rev. A **32**, 525 (1985); V. V. Konovalov, A. M. Raitsimring, Yu. D. Tsvetkov, and V. A. Benderskii, Chem. Phys. **93**, 163 (1985).

[4]For a comprehensive review of the problems in radiation physics, see M. Inokuti, in *Applied Atomic Collision Physics,* Vol. 4 of *Condensed Phases,* edited by S. Datz (Academic, New York, 1983), pp. 179–236.

[5]For a review see *Electron Beam Interactions in Solids for Microscopy, Microanalysis, and Microlithography,* edited by D. F. Kyser, H. Niedrig, D. E. Newbury, and R. Shimizu (Scanning Electron Microscopy, Inc., AMF O'Hare, Illinois, 1984).

[6]H. Ibach and D. L. Mills, *Electron Energy Loss Spectroscopy and Surface Vibrations* (Academic, New York, 1982).

[7]R. F. Willis and B. Feuerbacher, in *Photoemission and the Electronic Properties of Surfaces,* edited by B. Feuerbacher, B. Fitton, and R. F. Willis (Wiley, New York, 1978).

[8]J. B. Pendry, Phys. Rev. Lett. **45**, 1356 (1980).

[9]R. A. Fava, in *Treatise in Material Science and Technology,* edited by J. M. Schutz (Academic, New York, 1977), Vol. 10, Part B, pp. 677–740.

[10]L. Sanche and M. Michaud, Phys. Rev. B **30**, 6078 (1984); in *Resonances in Electron-Molecule Scattering van der Waals Complexes, and Reactive Chemical Dynamics,* edited by Donald G. Truhlar (American Chemical Society, Washington, D. C., 1984), pp. 211–228 and references cited therein.

[11]M. Michaud and L. Sanche, Phys. Rev. B **30**, 6067 (1984).

[12]L. Sanche, G. Perluzzo, and M. Michaud, J. Chem. Phys. **83**, 3837 (1985); R. Marsolais, M. Michaud, and L. Sanche, Phys. Rev. A **35**, 607 (1987).

[13]G. Bader, G. Perluzzo, L. G. Caron, and L. Sanche, Phys. Rev. B **26**, 6019 (1982); **30**, 78 (1984); L. G. Caron, G. Perluzzo, G. Bader, and L. Sanche, *ibid.* **33**, 3027 (1986).

[14]B. Plenkiewicz, P. Plenkiewicz, G. Perluzzo, and J.-P. Jay-Gerin, Phys. Rev. B **32**, 1253 (1985); J.-P. Jay-Gerin, B. Plenkiewicz, P. Plenkiewicz, G. Perluzzo, and L. Sanche, Solid State Commun. **55**, 1115 (1985).

[15]G. Perluzzo, L. Sanche, C. Gaubert, and R. Baudoing, Phys. Rev. B **30**, 4292 (1984); G. Perluzzo, G. Bader, L. G. Caron, and L. Sanche, Phys. Rev. Lett. **55**, 545 (1985).

[16]L. Sanche, Phys. Rev. Lett. **53**, 1638 (1984); L. Sanche and L. Parenteau, J. Vac. Sci. Technol. A **4**, 1240 (1986).

[17]G. Bader, J. Chiasson, L. G. Caron, M. Michaud, G. Perluzzo, and L. Sanche (unpublished).

[18]U. Fano and J. A. Stephens, Phys. Rev. B **34**, 438 (1986).

[19]C. J. Powell, Surf. Sci. **44**, 29 (1974).

[20]C. J. Tung, J. J. Lou, and S. W. Lin, Nucl. Instrum. Methods Phys. Res. B **16**, 83 (1986) and references cited therein; H. G. Paretzke, J. E. Turner, R. N. Hamm, H. A. Wright, and R. H. Ritchie, J. Chem. Phys. **84**, 3182 (1986) and references cited therein.

[21]R. L. Kurtz, N. Usuki, R. Stockbauer, and T. E. Madey, J. Electron. Spectrosc. and Relat. Phenom. **40**, 35 (1986).

[22]G. Seng and F. Linder, J. Phys. B **9**, 2539 (1976).

[23]T. Goulet, J.-P. Jay-Gerin, and J. P. Patau, J. Electron. Spectrosc. Relat. Phenom. **43**, 17 (1987).

[24]R. W. G. Wyckoff, *Crystal Structures,* 2nd ed. (Interscience, New York, 1963), p. 322.

[25]M. Michaud and L. Sanche, J. Vac. Sci. Technol. **17**, 274 (1980).

[26]C. Gaubert, R. Baudoing, Y. Gauthier, M. Michaud, and L. Sanche, Appl. Surf. Sci. **25**, 195 (1986).

[27]M. Michaud, L. Sanche, C. Gaubert, and R. Baudoing (unpublished).

[28]J. A. Venables, J. L. Seguin, J. Suzanne, and M. Bienfait, Surf. Sci. **145**, 345 (1984) and references cited therein; C. G. Shaw, S. C. Fain, Jr., and M. D. Chinn, Phys. Rev. Lett. **41**, 955 (1978); K. Horn, C. Mariani, and L. Cramer, Surf. Sci. **117**, 376 (1982) and references cited therein.

[29]K. Christmann and J. E. Demuth, Surf. Sci. **120**, 291 (1982); T. Engel, P. Bornemann, and E. Bauer, *ibid.* **81**, 252 (1979).

[30]O. G. Peterson, D. N. Batchelder, and R. O. Simmons, Phys. Rev. **150**, 703 (1966).

[31]L. E. Firment and G. A. Somorjai, Surf. Sci. **84**, 275 (1979).

[32]D. L. Doering and T. E. Madey, Surf. Sci. **123**, 305 (1982); P. A. Thiel, R. A. De Paola, and F. M. Hoffmann, J. Chem. Phys. **80**, 5326 (1984).

[33]E. Langenback, A. Spitzer, and H. Lüth, Surf. Sci. **147**, 179 (1984).

[34]For a review of nucleation and growth of thin molecular films, see J. A. Venables, G. D. T. Spiller, and M. Handbüken, Rep. Prog. Phys. **47**, 399 (1984); M. Bienfait, Surf. Sci. **162**, 411 (1985).

[35]A. H. Narten, C. G. Venkatesh, and S. A. Rice, J. Chem. Phys. **64**, 1106 (1976).

[36]T. C. Sivakumar, D. Schuh, M. G. Sceats, and S. A. Rice, Chem. Phys. Lett. **48**, 212 (1977).

[37]M. Michaud and L. Sanche, following paper, Phys. Rev. A **36**, 4684 (1987).

[38]C. Szmytkowski, Chem. Phys. Lett. **136**, 363 (1987) and private communication cited therein.

[39]E. Brüche, Ann. Phys. **1**, 93 (1929); V. F. Sokolov and Yu. A. Sokolova, Pis'ma Zh. Tekh. Fiz. **7**, 627 (1981) [Sov. Tech. Phys. Lett. **7**, 268 (1981)]; O. Sueoka, S. Mori, and Y. Katayama, J. Phys. B **19**, L373 (1986).

[40]K. Takayanagi, in *Electron-Molecule Collision,* edited by I. Shimamura and K. Takayanagi (Plenum, New York, 1984), Chap. 1.

[41]D. S. Belić, M. Landau, and R. I. Hall, J. Phys. B **14**, 175 (1981).

[42]A. Jain and D. G. Thompson, J. Phys. B **16**, L347 (1983).

[43]M. Watanabe, H. Kitamura, and Y. Nakai, in *Vacuum Ultraviolet Radiation Physics,* edited by E. E. Koch, R. Haensel, and C. Kunz (Pergamon, New York, 1974), p. 70.